Available online at www.sciencedirect.com
ScienceDirect
Journal of Photochemistry and Photobiology A: Chemistry 190 (2007) 169–176
Journal of Photochemistry and Photobiology A:Chemistry
www.elsevier.com/locate/jphotochem

Towards a quantum mechanical description of the photochemistry of dihalogens in rare gas matrices

Alexander Borowski, Oliver Kühn *

Institut für Chemie und Biochemie, Freie Universität Berlin, Takustr. 3, D-14195 Berlin, Germany

Available online 25 February 2007

Abstract

Using the semiempirical diatomics-in-molecules method we investigate the nonadiabatically coupled multidimensional potential energy surfaces for Br_2 in solid argon. The multidimensional nature of the nuclear motion is accounted for by defining two problem-specific large amplitude coordinates which are coupled to a set of harmonic oscillators in the spirit of a reaction surface model. This not only facilitates a compact description of anharmonicity, but also provides a means for a systematic extension towards more degrees of freedom. Taking the coupled B and C states as an example, two dominant linear vibronic coupling modes are identified giving rise to a minimum four-dimensional model for describing predissociation.

Keywords: Dihalogens; Rare gas matrix; Nonadiabatic couplings; Diatomics in molecules

1. Introduction

Although the violation of the Born-Oppenheimer approximation is at the heart of most photochemical and photobiological processes, a proper theoretical description still poses a considerable challenge. This already holds true, for instance, for small organic molecules in the gas-phase and even more so for complex biological systems [1]. In the latter case analysis and simulation of experimental data is faced by the large number of degrees of freedom and the necessity to invoke approximations from the very beginning. Therefore, it would be desirable to have at hand a system which shows many of the intricacies of nonadiabatic dynamics, but at the same time is amenable to a detailed theoretical and experimental study. It turns out that dihalogens in rare gas matrices – although seemingly simple – fulfill these criteria.

The study of the photophysics and photochemistry of these systems has a long history (for a review, see [2,3]). More recently, there has been considerable experimental interest in the quantum mechanical nature of the dynamics, triggered by ultrashort laser pulses. In particular Schwentner and coworkers unraveled a host of phenomena such as ultrafast spin-flip [4,5], generation of coherent zone-boundary phonons [6,7], or coherence transfer during collisions with the cage [8]. The issue of coherence versus decoherence has also been illuminated by Apkarian and coworkers [9]. The observation of long-lasting coherence triggered the question of controlling these simplest condensed phase systems by means of shaped laser pulses. Successful realization of laser control includes chirped pulse excitation which has been used to compensate for wave packet dispersion and thus to differentiate between the effects coming from the anharmonicity of the chromophore's potential and from matrix interactions [10]. In another experiment the use of wave packet interferometry allowed to prepare wave packets in an electronically excited state with well-defined chromophore-matrix coupling [11]. The mere possibility of this experiment provided the proof that electronic coherence is preserved on a time scale of about 600 fs for the exemplary case of the B ← X transition of Cl_2:Ar.

From the theoretical point of view these systems are considered prototypical for condensed phase situations [12] and a test ground for method development [13]. Much effort has been devoted to the description of nonadiabatic electronic transitions in classical trajectory simulations for the nuclei using the surface hopping approach [14–16]. This, however, cannot account for quantum effects in the nuclear motion. Here, semiclassical approximations have been pursued which retain phase information along classical trajectories [17–20]. Alternatively, mean-field type approaches such as the classically separable potential method have been applied [21,22]. Orig-

* Corresponding author. Tel.: +49 30 83855342; fax: +49 30 83854792.
E-mail address: ok@chemie.fu-berlin.de (O. Kühn).
URL: http://userpage.chemie.fu-berlin.de/~ok/ (O. Kühn).

1010-6030/$ – see front matter © 2007 Elsevier B.V. All rights reserved.
doi:10.1016/j.jphotochem.2007.02.024

inally developed for one-dimensional quantum propagations only, this method has recently been extended to include the quantum correlations between pairs of coordinates [23]. Restricting the simulations to short times, reduced dimensionality models typically including at most two degrees of freedom, have also been shown to provide valuable insight into the coherent nature of coupled electron-vibrational dynamics [24–26].

Concerning the calculation of potential energy surfaces (PES) the diatomics-in-molecules (DIM) method [27] presents a reasonable compromise between accuracy and numerical feasibility. Usually, the DIM-Hamiltonian is expressed in terms of the full valence state basis, which is likely to include more states than needed to simulate spectroscopic experiments where the accessible energy range is defined by the laser parameters. Recently, we have shown [28] that a reduced basis set representation of the DIM-Hamiltonian is possible, which refers to a specific energy and spatial range. The procedure was demonstrated for Br_2 in Ar and works as follows: expressed in the basis of Hund's case *c* molecular valence bond functions, the Hamiltonian for the isolated diatomic is block-diagonal and the effect of the matrix can be classified according to whether it introduces intra-symmetric or inter-symmetric coupling. Taking additionally the energetics of the gas-phase dissociation limits into account it was shown that a model including 17 electronic states is sufficient for proper simulation of B ← X excitation conditions.

The dynamics of electronic transitions is governed by specific nuclear motions. For instance, symmetry-breaking plays an important role as demonstrated experimentally for the predissociation of I_2 [29–31]. Such effects can in principle be described to some extent by nonadiabatic trajectory simulations (see, e.g., Refs. [32,33]). However, in the context of laser control of nuclear wave packets on coupled electronic PES a quantum model is mandatory. In the present paper we take the first step and develop an approach to determine a reduced but multidimensional model for Br_2:Ar covering the essential degrees of freedom targeted to a particular experimental situation, that is, the B ← X excitation and subsequent predissociation via the B–C state coupling. Thereby we extend our previous consideration of the manifold of electronic states [28] to include nuclear coordinates as well. In doing so we will build on the idea of a Taylor expansion of the PES in the vicinity of the crossings between different electronic states leading to a multimode vibronic coupling problem. This approach is well established [34–36] and has been extensively used for the simulation of the ultrafast dynamics of, for instance, pyrazine [37,38] or Jahn-Teller systems [39]. In order to cover also the anharmonic part of the PES the vibronic coupling expansion is combined with a two-dimensional reaction surface spanned by problem specific large amplitude coordinates.

2. Theoretical methods

2.1. The diatomics-in-molecules (DIM)-Hamiltonian

The semiempirical DIM-Hamiltonian has proven to be a rather successful compromise between accuracy and numerical effort in the calculation of coupled electronic PES for dihalogen rare-gas problems [5,7,14,15,28]. Introduced by Ellison [27] it is based on a semiempirical representation of interaction in terms of pair potentials which are parameterized using ab initio and experimental data. As far as dihalogens are concerned, accounting for the ^{2}P-terms of the halogen atoms leads to a total of 36 valence states forming the basis for a matrix representation of the DIM-Hamiltonian which reads for a general system X_2:Rg as follows:

$$\boldsymbol{H}_{\mathrm{el}}(\boldsymbol{R}) = \boldsymbol{V}^{\mathrm{X_2}}(\boldsymbol{R}_1, \boldsymbol{R}_2) + \boldsymbol{V}^{\mathrm{X-Rg}}(\boldsymbol{R}) + \boldsymbol{V}^{\mathrm{Rg-Rg}}(\boldsymbol{R}_3, \ldots, \boldsymbol{R}_N) \times \boldsymbol{I}_{36}. \quad (1)$$

Here, $\boldsymbol{V}^{\mathrm{X_2}}(\boldsymbol{R}_1, \boldsymbol{R}_2)$ is the diagonal matrix containing the energies of the isolated dihalogen, $\boldsymbol{V}^{\mathrm{X-Rg}}(\boldsymbol{R})$ the dihalogen–rare gas atom interaction expressed in the valence state bond basis, and $\boldsymbol{V}^{\mathrm{Rg-Rg}}(\boldsymbol{R}_3, \ldots, \boldsymbol{R}_N)$ is the pair interaction potential between the rare gas atoms. We have made the dependence on the nuclear coordinates explicit and defined $\boldsymbol{R} = (\boldsymbol{R}_1, \ldots, \boldsymbol{R}_N)$ using indices 1 and 2 for the dihalogen molecule.

2.2. Br_2 in Ar

Our focus is on the topology of the PES for the exemplary case of Br_2 in a double substitutional site in an Ar fcc lattice as shown in Fig. 1. For our discussion we will use the reduced DIM-Hamiltonian of Ref. [28] which contains all states having the $^2P_{3/2} + {}^2P_{3/2}$ gas-phase dissociation limit as well as the B-state which leads to $^2P_{3/2} + {}^2P_{1/2}$. The latter was constructed by combining ab initio data for the isolated Br_2 [40] with photoelectron spectroscopic data for the Br–Ar interaction [41]. For the parameterization of the Ar–Ar interaction we have used the Lennard-Jones parameters of Aziz [42]. The Br_2 was placed along the ⟨1 1 0⟩ direction in an orthorhombic box containing 698 Ar atoms (number of particles $N = 700$) and periodic boundary conditions have been applied. The equilibrium geometries for the X and B states to be discussed below were obtained by simulated annealing using a Nose–Hoover thermostate [43,44].

In Fig. 2 we show a one-dimensional cut of the diabatic electronic states along the Br–Br bond distance coordinate and for a frozen Ar lattice. Our fous will be on the B-state for which upon bond elongation one encounters other crossing states in the order

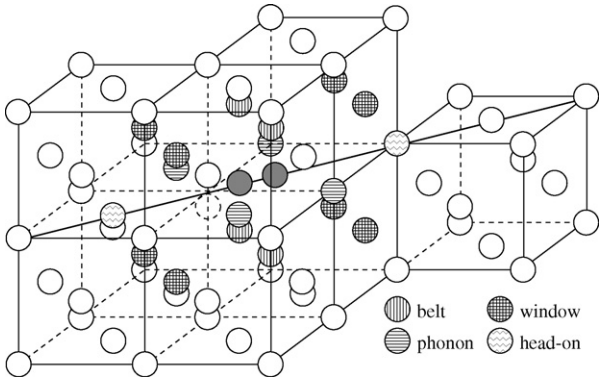

Fig. 1. Br_2 (filled circles) in Ar in a double substitutional lattice site in ⟨1 1 0⟩ direction. Adjacent cage atoms are classified as belt atoms, phonon atoms, window atoms, and head-on atoms.

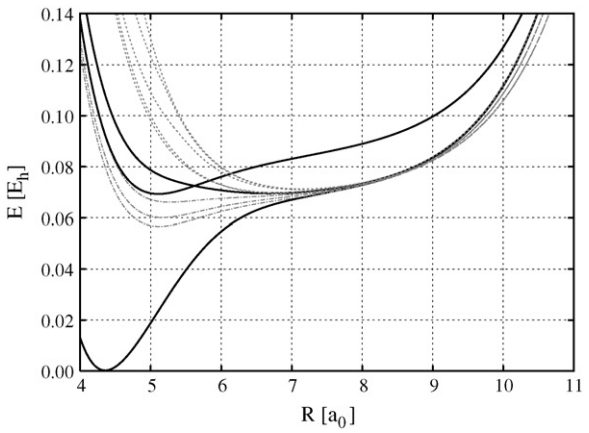

Fig. 2. One-dimensional diabatic potential energy curves along the Br–Br distance and for the case of Ar atoms fixed at the X-state equilibrium geometry. The target states which are considered in the present model are (solid lines) $X(0_g^+)$, $B(0_g^+)$, $C(1_u)$. Further we show the states which are bound ($A'(2_u)$, $A(1_u)$, $^3\Pi_u(0_u^-)$: dashed-dotted lines, labels in order of increasing energy) and dissociative ($^3\Pi_g(2_g)$, $a(1_g)$, $a'(0_g^+)$, $1^3\Sigma_u^+(0_u^-)$, $^3\Delta_u(3_u)$: dashed lines, labels in order of the state crossings with B state upon increasing Br–Br bond length) in the gas-phase case.

C, $^3\Pi_g$, a, a′, $1^3\Sigma_u^+$ and $^3\Delta_u$. Increasing the bond length beyond $9a_0$ the confining potential due to the matrix cage becomes visible. At this bond length the Br atoms have essentially passed through the first rectangular Ar window and are approaching the head-on atoms (see Fig. 1).

2.3. Reduced model Hamiltonians

The vibrational motions in the vicinity of the X-state minimum can be described in harmonic approximation which leads to the introduction of phonon modes $\{\mathbf{Q}_i\}$ with frequencies $\{\omega_i\}$ ($i = 1, \ldots, 3N-3$). For the present system these phonons are characterized by the density of states, $N(\omega)$, shown in Fig. 3. The phonon density of states has the typical form known for Ar crystals [45].

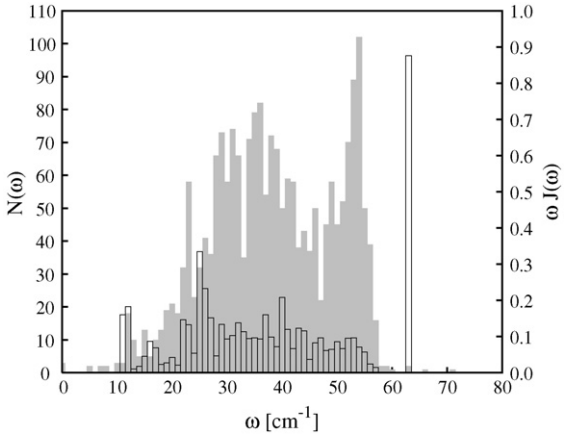

Fig. 3. Density of states $N(\omega)$ (grey bars) for the electronic ground state and spectral density $\omega J(\omega)$ (open bars) of the B ← X transition. Notice that we have not projected out the Br–Br motion, i.e., there will be a harmonic mode coupling at a frequency of about 320 cm^{-1} which correspond to the Br–Br bond vibration.

Concerning the coupling of these phonon modes to the electronic B ← X transition, the spectral density $J(\omega) = \sum_i g_i^2 \delta(\omega - \omega_i)$ is relevant. It weights each phonon mode by the dimensionless coupling strength g_i which represents the shift of the oscillator's minimum between the two states [12]. It is calculated from the force f_i acting on the ith ground state phonon mode Q_i in the B-state assuming a vertical transition, that is, $g_i = -f_i/\sqrt{2\hbar\omega_i^3}$ [12]. As can be seen from Fig. 3 the spectral density shows a pronounced coupling to a single mode at 63 cm^{-1} while the lower frequency part is more or less featureless.

Designing a reduced dimensionality model based on this information one is tempted to combine the anharmonic Br–Br coordinate with, e.g., this strongly coupled 63 cm^{-1} mode. Alternatively, one could select one or a subset of phonon modes for the reduced system according to their possible involvement in experiments. In fact, recent time-resolved spectroscopic data clearly revealed the specific role of particular vibrations of the matrix atoms in the vicinity of the diatomic (see, e.g., [7]). This procedure, however, is hampered by the fact that the choice is not unambiguous, also in view of approximate nature of the DIM which is not likely to give quantitative results. In any case, these approaches do not account for the anharmonicity of the Ar matrix vibrations which might play a role in particular for motions in the immediate surrounding of the chromophore.

One way of accounting for specific anharmonic vibrations is to construct a reduced dimensionality model, e.g., by combining the bond-distance coordinate with a matrix coordinate. In Ref. [24], for instance, the initial dynamics after photoexcitation of F_2 in Ar has been modeled by incorporating besides the F–F distance a coordinate which described the motion of the triangular Ar windows in ⟨l 1 1⟩ direction.

Following this strategy for the present case of Br_2 in Ar we show in Fig. 4 two-dimensional PES cuts along the Br–Br coordinate and the collective coordinate describing the belt and window atom motions, respectively, for the X-, B-, and C-state. Inspecting this figure one notices that there is a substantial coupling to both modes which includes at least linear and quadratic terms in the matrix coordinates. Furthermore, the potential along the matrix coordinate itself is not harmonic, that is, in the frame of a system-bath treatment these coordinates would have to be included into the "system". The conceptually most relevant problem, however, is that the present matrix coordinates have been heuristically chosen based on their anticipated role due to the proximity of the Ar atoms to the Br_2. Needless to say that this procedure would be hard to extend to more dimensions.

Therefore, it would be desirable to have a means for designing models which (i) capture some important part of the (anharmonic) PES in a compact form and (ii) whose dimensionality can be extended systematically. Both issues have to be considered in the context of a particular process under investigation. Here, we suggest to adapt a strategy which has been developed to describe intramolecular proton transfer reactions (see, e.g., [46]). In a nutshell, it involves the determination of two orthogonal large amplitude coordinates (LAC) (i.e. reaction coordinates) whose anharmonicity is fully accounted for. In a second step

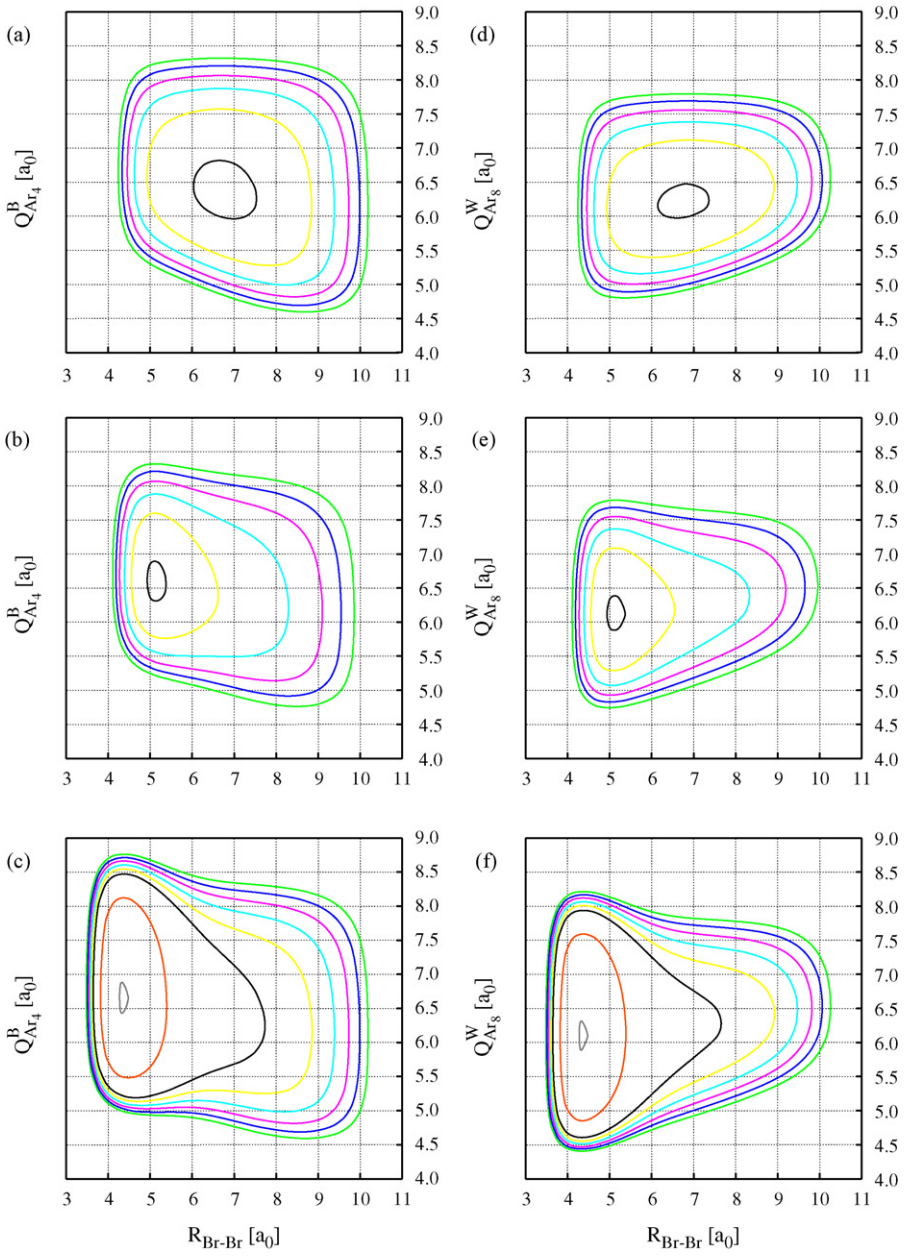

Fig. 4. Two-dimensional projections of the PES along the Br_2 bond distance and the belt coordinate (a–c) window coordinate (d–f) for states X, B, C (from bottom to top); coordinates defined perpendicular to the Br–Br bond axis. (Contours in E_h: 0.07, 0.08, 0.09, 0.10, 0.11, and 0.12 (a, b, d, and e), panels (c and f) include additional contours at 0.001 and 0.035.)

these LAC are coupled to the remaining degrees of freedom which are treated in harmonic approximation.

The choice of the first LAC is obvious, that is, we take the Br–Br bond distance:

$$\boldsymbol{\zeta}_R = \sqrt{\frac{M_{Br}}{2}}(R_{2,y} - R_{1,y})\boldsymbol{e}_y \tag{2}$$

as shown in Fig. 5a. Notice that the coordinate system is chosen such that the diatomic points along the y-direction (unit vector $\boldsymbol{e}_y$). Further, we will use mass-weighted coordinates in the following. As for the second reaction coordinate we will restrict our discussion on the electronic B-state. Thus we build the second coordinate from the mass-weighted difference vector Δ characterizing the equilibrium positions of the Ar atoms in the X- and the B-state minima $\boldsymbol{R}^{(X)}$ and $\boldsymbol{R}^{(B)}$, that is, $\Delta = \boldsymbol{M}^{1/2}(\boldsymbol{R}^{(B)} - \boldsymbol{R}^{(X)})$. Gram-Schmidt orthogonalization gives

$$\boldsymbol{\zeta}_{X\text{–}B} = \Delta - (\Delta, \boldsymbol{\zeta}_R)\boldsymbol{\zeta}_R \tag{3}$$

which is subsequently normalized. Displacements along both LAC vectors are defined with respect to $\boldsymbol{R}^{(X)}$. Motion along $\boldsymbol{\zeta}_{X\text{–}B}$ involves specific Ar atoms only as shown in Fig. 5b, this includes the collective displacement of the belt, window, phonon, and head-on atoms in the immediate surrounding of the diatomic. In this respect it resembles the combined effect of the intuitive coordinates described in Fig. 3. Notice that due to the symmetric deformation of the cage mapped out by this procedure, the LAC

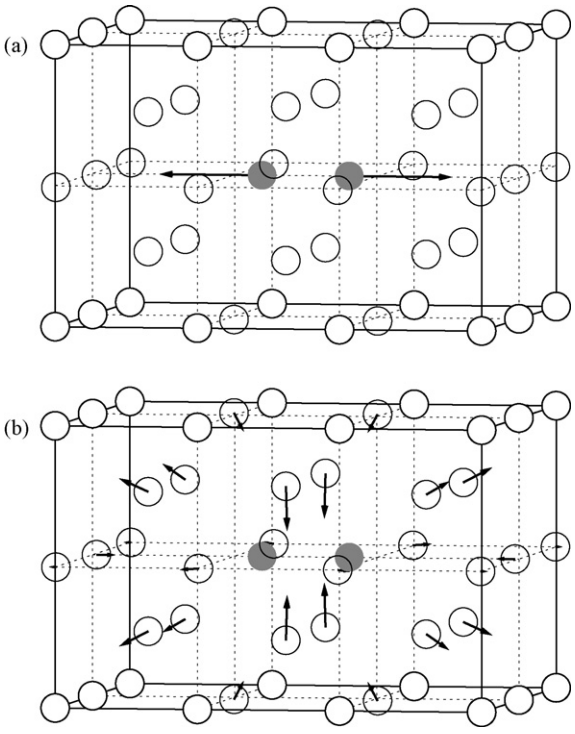

Fig. 5. Displacement vectors of the mass-weighted LAC defined in Eq. (2) (panel a) and (3) (panel b).

do not describe any displacement of the away from the ⟨1 1 0⟩ direction. Small amplitude librational type of motions of the Br_2 are nevertheless possible (cf. Fig. 9).

It is important to keep in mind that the choice of $\boldsymbol{\zeta}_{\mathrm{X–B}}$, Eq. (3), puts emphasis on the PES region in the vicinity of the B-state minimum. Thus, a priori it is not clear that it gives a meaningful description of the matrix for large Br–Br distances. In principle our approach is flexible enough to provide a check by adding another LAC appropriate for describing this region. To this end we have chosen a third geometry corresponding to the outer turning point of the Br–Br motion in the B-state at the Franck-Condon energy ($\sim 9a_0$) and a relaxed Ar matrix. It turns out that the vector pointing from the B-state minimum to this configuration is nearly parallel to $\boldsymbol{\zeta}_{\mathrm{X–B}}$, that is $\boldsymbol{\zeta}_{\mathrm{X–B}}$, shall provide a reasonable description also for this region of the PES.

Finally, we note that it is not guaranteed that the intrinsic reaction path from the Franck-Condon vertical transition geometry to the B-state minimum lies in the plane spanned by the LAC. However, this path is likely to be of no relevance for the description ultrafast dynamical processes our model is designed for.

2.4. Vibronic coupling

The LAC described in the previous paragraph are constructed such as to capture that part of the anharmonicity of the PES which is related to the symmetric deformation of the cage in the B-state. Therefore, it is reasonable to assume that the remaining orthogonal degrees of freedom can be approximated as harmonic oscillators coupled to the LAC. Since there is an electronic coupling of the B-state to a number of other states (cf. Fig. 2), it is suggestive to include these oscillator degrees of freedom in the context of vibronic coupling theory [1].

To identify the coupled normal modes we first diagonalized the mass-weighted second derivative matrix at the X-state PES minimum ($\boldsymbol{R} = \boldsymbol{R}_{\mathrm{ref}}$) under the condition that the three translations as well the two reaction coordinates have been projected out. The corresponding normal modes will be labeled as $\{\boldsymbol{q}_k\}$ with frequencies $\{\omega_k\}$ ($k = 1, \ldots, 3N-5$).

Casting the DIM-Hamiltonian (1) into the diabatic representation in terms of the Hund's case c valence bond basis $\{|a\rangle\}$ one obtains

$$H = \sum_a \left[\frac{\boldsymbol{P}^2}{2} + U_a(\boldsymbol{\zeta}_R, \boldsymbol{\zeta}_{\mathrm{X–B}}, \boldsymbol{q}) \right] |a\rangle\langle a| + \sum_{a \neq b} V_{ab}(\boldsymbol{\zeta}_R, \boldsymbol{\zeta}_{\mathrm{X–B}}, \boldsymbol{q}) |a\rangle\langle b| \quad (4)$$

where $\boldsymbol{P}$ denotes the (mass-weighted) momentum vector of all coordinates. Notice that the present use of orthogonal coordinates has the additional advantage that there appear no kinetic couplings. The diagonal PES introduced in Eq. (4) are given by

$$U_a(\boldsymbol{\zeta}_R, \boldsymbol{\zeta}_{\mathrm{X–B}}, \boldsymbol{q}) = V_{aa}^{\mathrm{Br_2}}(\boldsymbol{\zeta}_R) + V_{aa}^{\mathrm{Br–Ar}}(\boldsymbol{\zeta}_R, \boldsymbol{\zeta}_{\mathrm{X–B}}, \boldsymbol{q}) + V^{\mathrm{Ar–Ar}}(\boldsymbol{\zeta}_{\mathrm{X–B}}, \boldsymbol{q}) \quad (5)$$

Adopting a harmonic expansion of these diagonal elements in terms of $\boldsymbol{q}$ yields shifted oscillator PES where the particular strength of coupling to the electronic transition could be described by an appropriate spectral density (cf. Fig. 3 for the fully harmonic case). For the off-diagonal elements we have

$$V_{ab}(\boldsymbol{\zeta}_R, \boldsymbol{\zeta}_{\mathrm{X–B}}, \boldsymbol{q}) = V_{ab}^{\mathrm{Br–Ar}}(\boldsymbol{\zeta}_R, \boldsymbol{\zeta}_{\mathrm{X–B}}, \boldsymbol{q}) \quad (6)$$

In the spirit of the harmonic approximation, the dependence of these matrix element on the normal mode coordinates will be obtained via a Taylor expansion of lowest order [1], that is

$$V_{ab}^{\mathrm{Br–Ar}}(\boldsymbol{\zeta}_R, \boldsymbol{\zeta}_{\mathrm{X–B}}, \boldsymbol{q}) = V_{ab}^{\mathrm{Br–Ar}}(\boldsymbol{\zeta}_R, \boldsymbol{\zeta}_{\mathrm{X–B}}, \boldsymbol{q})|_{R_{\mathrm{ref}}} + \boldsymbol{F}_{ab}(\boldsymbol{\zeta}_R, \boldsymbol{\zeta}_{\mathrm{X–B}})\boldsymbol{q} \quad (7)$$

Here, we defined the electronic matrix elements of the first derivative with respect to the interaction, projected onto the respective normal modes:

$$\boldsymbol{F}_{ab}(\boldsymbol{\zeta}_R, \boldsymbol{\zeta}_{\mathrm{X–B}}) = \nabla_R V_{ab}^{\mathrm{Br–Ar}}(\boldsymbol{R})|_{R_{\mathrm{ref}}} \boldsymbol{M}^{-1/2} \boldsymbol{L} \quad (8)$$

where $\boldsymbol{L}$ is the normal mode transformation matrix and $\boldsymbol{M}$ is the diagonal mass-matrix.

3. Results

3.1. Analysis of reaction coordinates

While the meaning of the LAC $\boldsymbol{\zeta}_R$, Eq. (2), is obvious, the appreciation of the collective coordinate $\boldsymbol{\zeta}_{\mathrm{X–B}}$, Eq. (3), requires more attention. We have pointed out its characteristics in terms of displacements of Ar atoms of the matrix cage (cf. Fig. 5b), however, a more detailed view is provided by projecting this

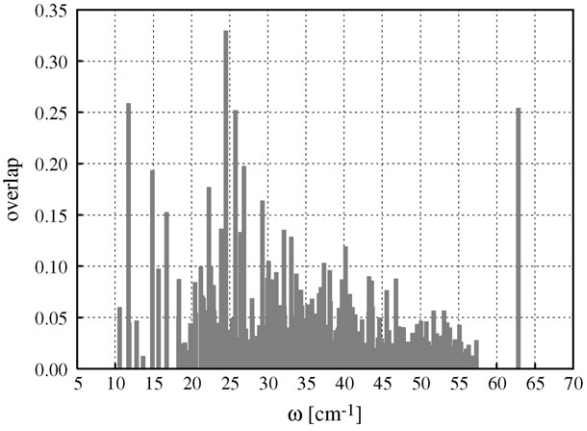

Fig. 6. Projection of the ground state normal modes (cf. Fig. 3) onto the large-amplitude displacement ζ_{X-B}.

coordinate onto the *total* (only translations projected out) set of normal modes,$\{\mathbf{Q}_i\}$, of the X-state PES minimum. The result, that is, the scalar product ($\boldsymbol{\zeta}_{X-B}$, $\mathbf{Q}_i$), is shown in Fig. 6 from which it becomes clear that this coordinate really involves contributions from many symmetry-preserving normal modes covering an essential part of the whole phonon spectrum. One should emphasize that this hints to a minor drawback of this compact description of the coupling to the matrix, that is, an additional effort is necessary, if an interpretation in terms of specific phonon modes is required. Finally, it is interesting to compare Fig. 6 with the spectral density shown in Fig. 3. Obviously, $\boldsymbol{\zeta}_{X-B}$ resembles the totally symmetric part of the linear coupling modes in the Franck-Condon region.

3.2. Potential energy surface cuts

In the following we focus exclusively on the scenario of an excitation from the X to the coupled B and C states. Fig. 7 shows the 2D cuts of the three diabatic PES for the case that the orthogonal normal modes are frozen at their X-state equilibrium positions $U_a(\boldsymbol{\zeta}_R, \boldsymbol{\zeta}_{X-B}, \boldsymbol{q} = 0)$. First, we notice that the PES in all three states is tilted towards larger $\boldsymbol{\zeta}_{X-B}$ upon increasing $\boldsymbol{\zeta}_R$. This is in accord with the general picture modification of the cage upon Br–Br bond stretching already encountered in Fig. 4. A related observation is that the minimum of the PES shifts towards larger $\boldsymbol{\zeta}_R$ in the B-state as already seen in Fig. 2. However, it also shifts towards larger $\boldsymbol{\zeta}_{X-B}$ implying that, for instance, the belt and window atoms move inward and outward, respectively, in response to the Br–Br bond elongation. Second, we notice that the shape of the PES changes as well, e.g., the vicinity of the minima the $\boldsymbol{\zeta}_{X-B}$ motion is softer in the B state. Due to the repulsive potential provided mostly by the head-on atoms, the C-state becomes bound as well (cf. Fig. 2). Notice that the diabatic C and X states are essentially degenerate in the region of the minimum.

3.3. Analysis of vibronic coupling

Instead of the diabatic picture of the B and C states PES one can follow the lowest state on the PES for $\boldsymbol{q} = 0$ to visualize the topology of the crossing region. This is shown in Fig. 8. Consid-

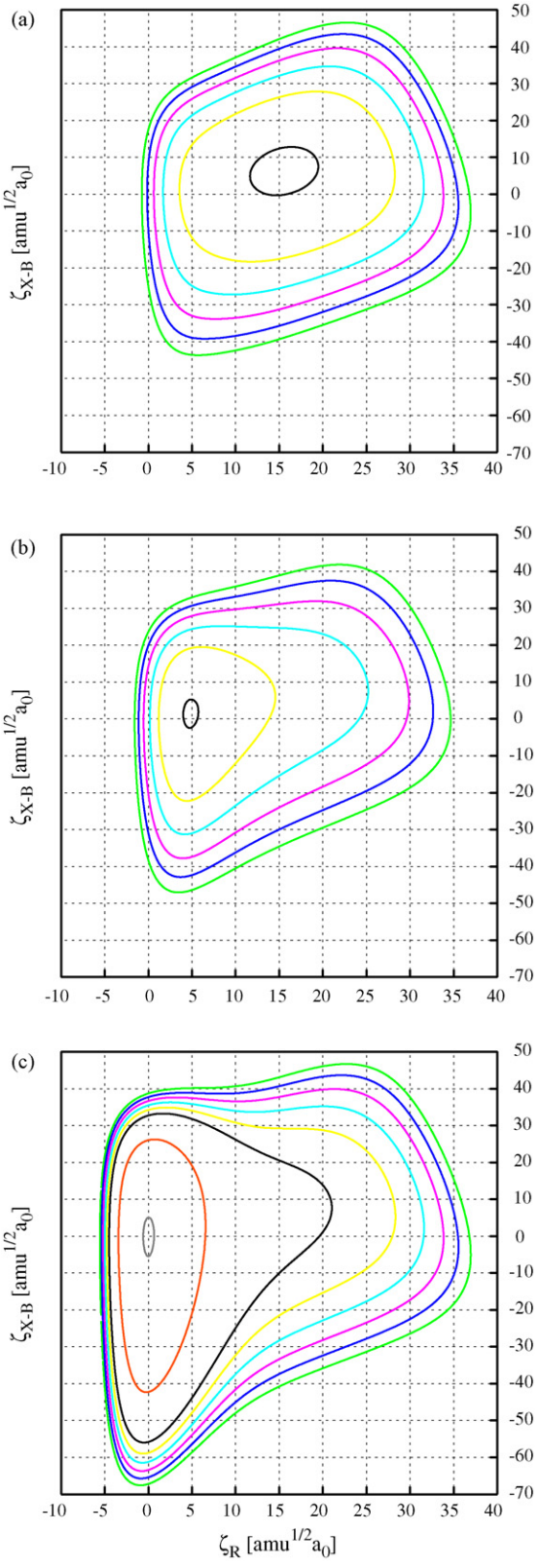

Fig. 7. Diabatic PES cuts along the LAC for the X, B, and C states (from bottom). Contour lines in E_h at 0.069, 0.08, 0.09, 0.10, 0.11, and 0.12 panels (a–c), additional contours at 0.001 and 0.035 in panel (c).

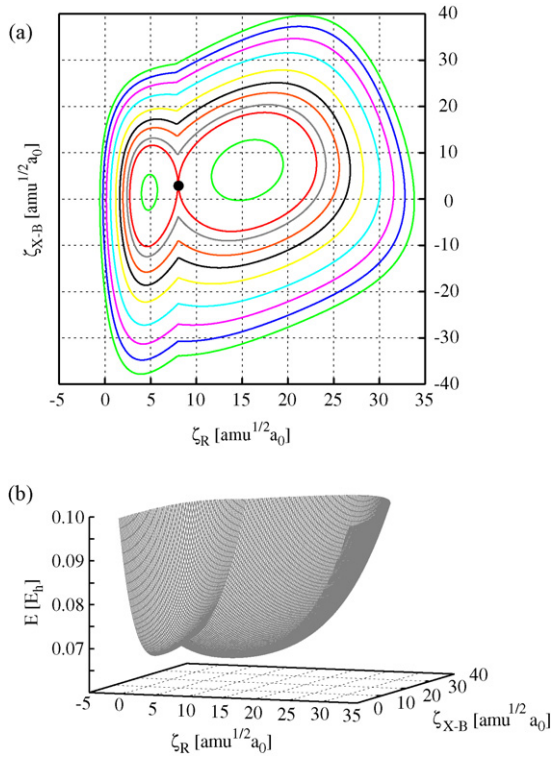

Fig. 8. Lowest energy diabatic PES for the B and C states. (a) Contours in E_h at 0.0693, 0.0719, 0.0730, 0.0750, 0.0770, 0.080, 0.085, 0.09, 0.095, and 0.1. The black dot marks the minimum point along the crossing seam. (b) Same as panel (a), but in a three-dimensional view.

ering a rectangular cut-out of the crystal along the ⟨110⟩ direction of the Br–Br bond axis one has an overall D_{2h} symmetry. This symmetry is preserved on the whole PES spanned by the reaction coordinates. As a consequence the B and C state which are of 0_u^+ and 1_u symmetry in the isolated molecule intersect along a crossing seam. The lowest point along this seam is indicated by a dot in Fig. 8a.

In order to identify the coupling modes we have calculated the vector of matrix elements $\boldsymbol{F}_{BC}(\boldsymbol{\zeta}_R, \boldsymbol{\zeta}_{X\text{–}B})$ Eq. (8) at the minimum of the crossing seam. The result is shown in Fig. 9a. It turns out that two modes are strongly coupled while an almost continuous distribution of modes stretching from 7 to 57 cm^{-1} couples only weakly. As expected on group theoretical grounds the strongly coupled modes are of B_{2g} (63 cm^{-1}) and B_{3g} (60 cm^{-1}) symmetry. Their displacement vectors depicted in Fig. 9b and c show how motion along these modes reduces the nuclear cage symmetry, hence splitting the degeneracy of the PES in Fig. 8. Interestingly, the B_{3g} mode involves a libration-type motion of Br_2 in the cage.

For the construction of a PES it is necessary to have at hand the functional dependence of $\boldsymbol{F}_{BC}(\boldsymbol{\zeta}_R, \boldsymbol{\zeta}_{X\text{–}B})$ and especially to determine whether the coupling pattern with two dominating modes in Fig. 9a changes when moving away from the minimum point on the seam. We have investigated this issue numerically and observed that within a range of up to 2.5 eV above this minimum point the coupling pattern does not change significantly. Further, the coordinate dependence of $\boldsymbol{F}_{BC}(\boldsymbol{\zeta}_R, \boldsymbol{\zeta}_{X\text{–}B})$ along the seam is only modest.

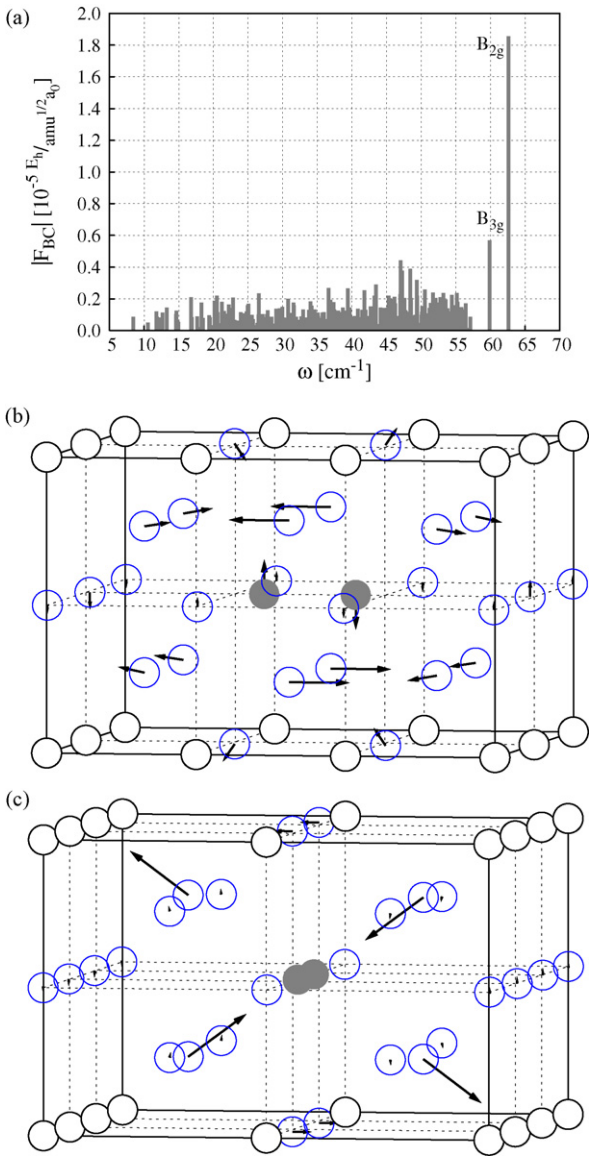

Fig. 9. (a) Projection of off-diagonal elements of the vibronic coupling Hamiltonian onto the normal modes which are orthogonal to the LAC, Eq. (8). The displacement vectors of the two strongest coupling modes are shown in panels (b) (B_{3g}) and (c) (B_{2g}).

Comparing Fig. 9 with the spectral density in Fig. 3 we need to emphasize the following points: incidentally in both cases there is a dominant peak around 63 cm^{-1}. However, while the 63 cm^{-1} mode in Fig. 3 is totally symmetric, it is of B_{2g} symmetry in Fig. 9. It should be noted, that within the LAC model one still finds a totally symmetric mode which dominantly couples in the Franck-Condon region (not shown). Its character is similar to the full model in Fig. 3, but its frequency is shifted to around 61 cm^{-1}.

4. Summary

The theoretical description of electronic and vibrational coherence in the time evolution after ultrafast photoexcitation with a specially designed laser field requires a full quantum

treatment. In the present work we have discussed the construction of an appropriate Hamiltonian based on the semiempirical DIM method. Introducing anharmonic large amplitude coordinates supplemented by orthogonal harmonic modes we have essentially a method which provides a problem-adapted vibronic coupling Hamiltonian whose dimensionality can be tuned according to the desired degree of sophistication of the model. This holds true in particular as far as the number of coupled oscillator modes is concerned. However, one could also consider to incorporate second order terms in the expansion of the vibronic coupling or to include anharmonicity with respect to the oscillator's PES. For the coupled B–C state dynamics of Br_2 in Ar which may involve the laser control of predissociation we have found that besides the two LAC, two symmetry-lowering harmonic modes play the role of the dominant linear coupling modes. Additionally, there is a dense spectrum of modes which provide a much weaker coupling.

The model presented here is well-suited for implementation within the multiconfiguration time-dependent Hartree (MCTDH) wave packet propagation scheme [47]. Starting from a four-dimensional model one could successively incorporate representative modes from the dense spectrum or include their effect within a density matrix description. The detail of information obtainable this way would not only keep up with the experimental data, but could also be interesting for comparing with approximate semiclassical methods.

In summary, although a diatomic in a rare gas matrix looks like a simple setup it contains all the complications of non-Born-Oppenheimer quantum dynamics and therefore constitutes a valuable testing ground for both experiment and theory.

Acknowledgments

This work has been supported by the Deutsche Forschungsgemeinschaft (Sfb450). We are grateful to H. Ibrahim (Berlin) for carefully reading the manuscript.

References

[1] W. Domcke, D.R. Yarkony, H. Köppel, Conical Intersections, World Scientific, New Jersey, 2004.
[2] V.A. Apkarian, N. Schwentner, Chem. Rev. 99 (1999) 1481.
[3] M. Bargheer, et al., in: O. Kühn, L. Wöste (Eds.), Analysis and Control of Ultrafast Photoinduced Reactions, Springer, Heidelberg, 2007, p. 257.
[4] M. Bargheer, M.Y. Niv, R.B. Gerber, N. Schwentner, Phys. Rev. Lett. 89 (2002) 108301.
[5] M. Bargheer, R.B. Gerber, M.V. Korolkov, O. Kühn, J. Manz, M. Schröder, N. Schwenter, Phys. Chem. Chem. Phys. 4 (2002) 5554.
[6] M. Gühr, M. Bargheer, N. Schwentner, Phys. Rev. Lett. 91 (2003) 085504.
[7] M. Fushitani, N. Schwentner, M. Schröder, O. Kühn, J. Chem. Phys. 124 (2006) 024505.
[8] M. Bargheer, M. Gühr, N. Schwentner, Israel. J. Chem. 44 (2004) 9.
[9] D. Segale, M. Karavitis, E. Fredj, V.A. Apkarian, J. Chem. Phys. 122 (2005) 111104.
[10] M. Gühr, H. Ibrahim, N. Schwentner, Phys. Chem. Chem. Phys. 6 (2004) 5353.
[11] M. Fushitani, M. Bargheer, M. Gühr, N. Schwentner, Phys. Chem. Chem. Phys. 7 (2005) 3143.
[12] V. May, O. Kühn, Charge and Energy Transfer Dynamics in Molecular Systems, 2nd revised and enlarged edition, Wiley–VCH, Weinheim, 2004.
[13] P. Jungwirth, R.B. Gerber, Chem. Rev. 99 (1999) 1583.
[14] G. Chaban, R.B. Gerber, M.V. Korolkov, J. Manz, M.Y. Niv, B. Schmidt, J. Phys. Chem. A 105 (2001) 2770.
[15] V.S. Batista, D.F. Coker, J. Chem. Phys. 106 (1997) 6923.
[16] I.H. Gersonde, H. Gabriel, J. Chem. Phys. 98 (1993) 2094.
[17] O. Kühn, N. Makri, J. Phys. Chem. A 103 (1999) 9487.
[18] M. Ovchinnikov, V.A. Apkarian, G.A. Voth, J. Chem. Phys. 114 (2001) 7130.
[19] M. Ovchinnikov, V.A. Apkarian, J. Chem. Phys. 108 (1998) 2277.
[20] M.L. Brewer, J.S. Hulme, D.E. Manolopoulos, J. Chem. Phys. 106 (1997) 4832.
[21] P. Jungwirth, E. Fredj, R.B. Gerber, J. Chem. Phys. 107 (1997) 8963.
[22] P. Jungwirth, R.B. Gerber, J. Chem. Phys. 102 (1995) 6064.
[23] H.H. Eshet, M.A. Ratner, R.B. Gerber, Chem. Phys. Lett. 431 (2006) 199.
[24] M.V. Korolkov, J. Manz, Z. Phys. Chem. 217 (2003) 115.
[25] A.B. Alekseyev, M.V. Korolkov, O. Kühn, J. Manz, M. Schröder, J. Photochem. Photobiol. A 180 (2006) 262.
[26] S.F. Alberti, J. Echave, V. Engel, N. Halberstadt, J.A. Beswick, J. Chem. Phys. 113 (2000) 1027.
[27] F.O. Ellison, J. Am. Chem. Soc. 85 (1963) 3540.
[28] A. Borowski, O. Kühn, Theor. Chem. Acc. 117 (2007) 521.
[29] G. Flachenecker, V.A. Ermoshin, V. Engel, R. Neder, G. Wirnsberger, A. Materny, Phys. Chem. Chem. Phys. 5 (2003) 865.
[30] V.A. Ermoshin, G. Flachenecker, A. Materny, V. Engel, J. Chem. Phys. 114 (2001) 8132.
[31] R. Zadoyan, M. Sterling, M. Ovchinnikov, V.A. Apkarian, J. Chem. Phys. 107 (1997) 8446.
[32] N. Yu, C.J. Margulis, D.F. Coker, J. Phys. Chem. B 105 (2001) 6728.
[33] V.S. Batista, D.F. Coker, J. Chem. Phys. 105 (1996) 4033.
[34] L.S. Cederbaum, W. Domcke, Adv. Chem. Phys. 36 (1977) 205.
[35] L.S. Cederbaum, W. Domcke, H. Köppel, W. von Niessen, Chem. Phys. 26 (1977) 169.
[36] H. Köppel, W. Domcke, L.S. Cederbaum, Adv. Chem. Phys. 57 (1984) 59.
[37] W. Domcke, G. Stock, Adv. Chem. Phys. 100 (1997) 1.
[38] A. Raab, G.A. Worth, H.D. Meyer, L.S. Cederbaum, J. Chem. Phys. 110 (1999) 936.
[39] S. Mahapatra, V. Vallet, C. Woywod, H. Köppel, W. Domcke, Chem. Phys. 304 (2004) 17.
[40] Y. Asano, S. Yabushita, Chem. Phys. Lett. 372 (2003) 348.
[41] I. Yourshaw, Y. Zhao, D.M. Neumark, J. Chem. Phys. 105 (1996) 351.
[42] R.A. Aziz, J. Chem. Phys. 99 (1993) 4518.
[43] S. Nose, Mol. Phys. 53 (1984) 255.
[44] W. Hoover, Phys. Rev. A 31 (1985) 1695.
[45] Y. Fujii, N.A. Lurie, R. Pynn, G. Shirane, Phys. Rev. B 10 (1974) 3647.
[46] K. Giese, M. Petković, H. Naundorf, O. Kühn, Phys. Rep. 430 (2006) 211.
[47] H.-D. Meyer, G.A. Worth, Theor. Chem. Acc. 109 (2003) 251.